Molecular Viewpoint on the Crystal Growth Dynamics Driven by Solution Flow

Dominique Maes and James F. Lutsko*

Cite This: https://dx.doi.org/10.1021/acs.cgd.9b01434

Read Online

ACCESS | Metrics & More | Article Recommendations | Supporting Information

ABSTRACT: Standard solid-on-solid models of crystal growth represent the appearance and disappearance of molecules on the crystal surface as stochastic events. Here, in order to model more realistically the growth of crystals from solution, we introduce a dynamic model of the fluid in contact with the crystal surface and in this way account explicitly for mass transport in the solution. We present our hybrid model and establish its relation to standard SOS simulations while demonstrating explicit effects of mass transport that are usually ignored in SOS simulations. We then introduce flow in the solution in directions parallel to the crystal surface and observe dramatic effects on crystal growth for flows perpendicular to the step front as well as for flows parallel to the step. In order to understand the latter, quite unexpected feature, we study the effect of flow on isolated islands on a crystal surface and show that flow in the solution can induce spontaneous movement of 2D islands on the crystal surface.
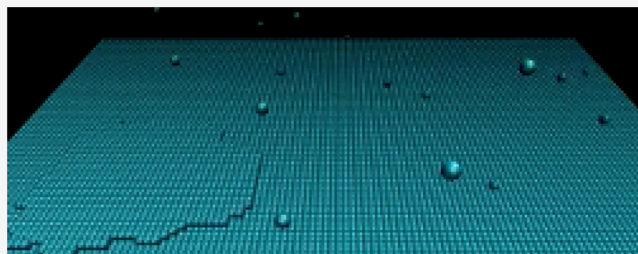
INTRODUCTION

Crystallization is a central process in materials science, engineering, and pharmacy. Many crystal growth processes involve fluid flows such as the continuously operated crystallizers used to produce crystals on an industrial scale and microfluidic devices, which are powerful tools for high-throughput experimentation and flow-/droplet-based crystallization and which offer a rich variety of solution flow geometries. Numerous experimental and theoretical results indicate that the flow increases the nucleation rate,[1−4] whereas the results for crystal growth are inconclusive. For *in situ* crystal growth studies biological macromolecules are often used as model systems because their large size enables molecular resolution of the surface features (e.g., using AFM[5−7] or confocal microscopy[8−10]) and the rate of the advancement of elementary steps can be used as a fundamental quantitative proxy of crystal growth.[11,12] *In situ* measurements of growing lysozyme crystals in forced flow using high-resolution interferometry,[13−16] microfluidics,[17,18] and LCM-DIM[19] showed that the effect of flow on growth is a complex picture depending on many factors such as the supersaturation, the presence of impurities, and even the growth mode. Moreover, the interaction between single steps has been shown to be affected by flow.[20]

Simulations can be a helpful tool to understand a physical phenomenon and to support experimental observations. Numerous macroscopic modeling studies have been performed to better understand crystal growth (see ref 21, for example). At the molecular level, beginning with the work of Gilmer and Bennema,[22] crystal growth has long been studied by means of simple kinetic Monte Carlo (kMC) models (see also ref 23).

This has led to important insights such as the role of impurities in blocking step growth[24] and in the formation and growth of supersteps.[25,26] The ability to visualize the simulated crystal growth process is valuable for a comprehensive understanding of the growth process and the clarification of the underlying physics. The aim of the work presented here is to extend the standard simulation models so as to explicitly represent fluid flow and mass transport above a growing crystal surface. The proposed model is illustrated by considering the growth of a single elementary step in the presence of constant flow parallel to the crystal face. More realistic, complex flows as well as the effect of impurities, the presence of multiple steps, etc. will be considered in a later work.

In the following, we first present the algorithm underlying our proposed model. Because the simulations include a finite volume above the crystal surface, various new physical effects must be taken into account such as the fact that the supersaturation at the crystal surface differs from that applied at the top of the simulation cell and can vary as the crystal grows and so these novel effects are discussed and characterized theoretically. This is followed by our illustrative simulations using an implementation of the algorithm in C++ with typical running times on the order of 120 h (typically,

twice as long as an equivalent SOS simulation). We first present step growth with no flow and then in the presence of flow for the case of a very simple uniform flow. Interestingly, we find that the rate of step growth as well as step morphology is affected by flows parallel to the step fronts and not just those perpendicular to the step as might be expected. Finally, a novel effect of flow on the behavior of small islands on an otherwise flat crystal surface is presented, followed by our conlusions.

DESCRIPTION OF THE ALGORITHM

Standard SOS Algorithm. It is useful to first recall the standard solid-on-solid (SOS) algorithm. In this model, there are no vacancies within the crystal so that each site on a (001) surface can be viewed as the topmost of a column of molecules extending down to some substrate. The crystal is therefore completely characterized by specifying for each location in the $x-y$ plane the height of the column of molecules at that position (see Figure 1). Assuming N_x sites in the x direction
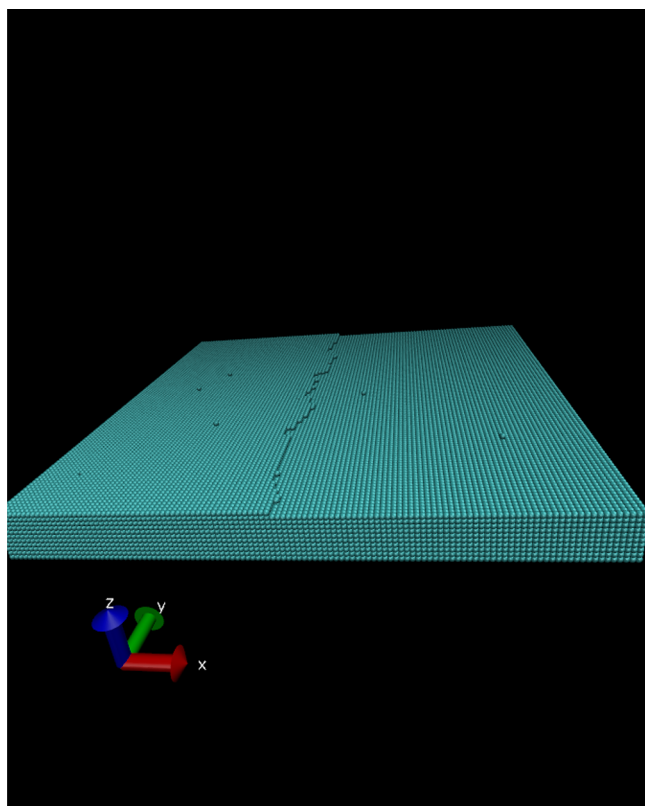
Figure 1. Image from an SOS simulation showing a partially completed surface layer.

and N_y in the y direction, the crystal can be represented as an array $\mathbf{H}$ of dimensions $N_x \times N_y$ in which the element H_{ij} is the height of the crystal at the site $x = i$ and $y = j$.

Molecules can form bonds of energy $-\varepsilon < 0$ with their nearest neighbors. Thus, in the interior of the crystal, each molecule participates in six bonds, giving a total energy per molecule in the crystal of -3ε. Only surface molecules have higher energy: the energy of a molecule at the surface site i, j will be denoted E_{ij} and it is determined simply by counting the number of nearest-neighbor bonds. For example, an adatom sitting on an otherwise flat surface will have only one nearest neighbor (the one directly below it) and will therefore have

energy $-\varepsilon/2$ since each bond is shared between the two neighbors.

The crystal is imagined to be in contact with a solution containing the molecules that can attach to the surface: similarly, the molecules on the surface can detach and enter the solution. The molecules in solution are modeled as having a constant energy μ (the chemical potential) so that they are in equilibrium with the molecules in the crystal for the chemical potential $\mu_{eq} = -3\varepsilon$. The crystal grows when it is energetically more favorable for molecules to move from solution into the crystal: i.e., when $\Delta\mu \equiv \mu - \mu_{eq} > 0$.

In the standard SOS model, the solution is treated implicitly, as discussed below. However, to properly account for the thermodynamics, the total system should be imagined to be the crystal, represented by the array $\mathbf{H}$, and a (large) number N of molecules in solution, each having energy μ. We will therefore denote the *total* system as $\mathbf{S} = (\mathbf{H}, N)$. For example, if one starts with $\mathbf{S}$ and a molecule attaches to the surface at site i, j from solution, then the new system will be $\mathbf{S}' = (\mathbf{H}', N - 1)$ where $H_{lk}' = H_{lk} + \delta_{il}\delta_{jk}$.

The kinetic Monte Carlo dynamics depend on first defining rate constants for molecules to attach to the surface (from solution) and for them to detach from the surface and go into solution. In general, these depend on the surface site under consideration, and so we write them as r_{ij}^+ and r_{ij}^-, respectively, for attachment and detachment at surface site i, j. The only requirement is that they obey a detailed balance so that the model has an equilibrium state. Let a possible transition of the system take the system $\mathbf{S}$ to a modified system $\mathbf{S}'$: then a detailed balance requires that the rate for this transition, $r(\mathbf{S} \to \mathbf{S}')$, and that for the reverse transition, $r(\mathbf{S}' \to \mathbf{S})$, satisfy $r(\mathbf{S} \to \mathbf{S}')/r(\mathbf{S}' \to \mathbf{S}) = \exp(-\beta(E(\mathbf{S}') - E(\mathbf{S})))$ where $E(\mathbf{S})$ is the total energy of the system $\mathbf{S}$. If the crystal energy (sum of bonds) is denoted $E_c(\mathbf{H})$, then $E(\mathbf{S}) = E_c(\mathbf{H}) + N\mu$ and $E(\mathbf{S}') - E(\mathbf{S}) = E_c(\mathbf{H}') - E_c(\mathbf{H}) + (N' - N)\mu$. For the particular cases of interest here, adding a molecule at the position i, j on the surface will involve a change in energy of $-n_{ij}\varepsilon - \mu$, where n_{ij} is the number of newly formed bonds. Similarly, removing the atom at position i, j will involve an energy change that is the negative of this quantity. Thus, one can take, for example, the rate for adding an atom at position i, j to be $r_{ij}^+ = \nu_0 e^{\beta\mu}$, where ν_0 is a frequency with units of inverse time (the so-called "attempt frequency") and the rate to remove an atom at position i, j to be $r_{ij}^- = \nu_0 e^{-n_{ij}\beta\varepsilon}$ so that the ratio is $r_{ij}^+/r_{ij}^- = e^{\beta(\mu+n_{ij}\varepsilon)}$. We refer to this choice as "simple probabilities". Alternatively, the standard Metropolis algorithm rates are $r_{ij}^+ = \nu_0 \min(1, e^{\beta(\mu+n_{ij}\varepsilon)})$ and $r_{ij}^- = \nu_0 \min(1, e^{\beta(-n_{ij}\varepsilon-\mu)})$, which gives the same ratios. In this paper, we use the first choice.

Once the rates have been specified, an elementary step in the algorithm consists of randomly choosing one of the $N_x \times N_y$ surface sites and randomly choosing one of three possible actions on the basis of their relative rates. To do this, we introduce a parameter r_0, which is specified below, and choose one of the following: (1) add a new molecule at that site with probability r_{ij}^+/r_0, (2) remove the molecule at that site with probability r_{ij}^-/r_0, and (3) do nothing (with probability $1 - r_{ij}^+/r_0 - r_{ij}^-/r_0$). The parameter r_0 must be chosen so that $r_{ij}^\pm/r_0 \leq 1$ for all possible cases and otherwise is, ideally, as small as possible to minimize the number of times that nothing happens. For example, using the simple probabilities, one has $r_{ij}^+ = \nu_0 e^{\beta\mu}$ and $r_{ij}^- = \nu_0 e^{\beta E_{ij}} \leq \nu_0 e^{-\beta\varepsilon}$ since any molecule on the surface will have at least one bond. Thus, one can take $r_0 = \nu_0 \max(e^{\beta\mu}, e^{-\beta\varepsilon})$. Since there are two possible events associated

with each surface site, the total number of possible events is $\mathcal{N} = 2N_xN_y$ and the resulting kMC algorithm is as follows:

- Select one of the $\mathcal{N}$ possible events randomly: let the selected site be i, j and the rate for the event be r_{ij}.
- Execute the event with probability r_{ij}/r_0.
- Increment the time by $t \rightarrow t + \delta t$ where $\delta t = \frac{1}{2N_xN_yr_0}$
- Has the stopping criterion been achieved? If yes, stop; if no, go to step 1.

Boundary Conditions. The simplest boundary conditions are periodic in the $x-y$ plane so that the points $H_{N_x+1,j} = H_{1j}$ and $H_{0j} = H_{N_xj}$ are for all values of j and, similarly, $H_{iN_y+1} = H_{i1}$ and $H_{i,0} = H_{i,N_x}$ are for all i. However, with periodic boundaries, it is not possible to have steady-state step growth: once a partially complete surface layer (as shown in Figure 1) is completed, the crystal surface is perfect and ceases to grow. To maintain steady-state growth, stepped periodic boundaries are used whereby (for the geometry in Figure 1 with the step parallel to the y axis and growing in the x direction) one sets $H_{N_x+1,j} = H_{1j} + 1$ and $H_{0j} = H_{N_xj} - 1$ while keeping ordinary periodicity in the y direction.

Mapping to Real Units. To give an example of how abstract parameters such as ε and μ could be fixed in a real system, we consider the mapping to lysozyme. Although, like most substances, lysozyme does not form a simple cubic phase, we note that Chernov[27] gives the areas of the faces of the unit cells in the various stable crystals (tetragonal, orthorhombic, and monoclinic) ranging from 8 to 60 nm^2 with a median of about 20 nm^2, which translates into a cubic lattice constant of about $a = 4.5$ nm. Similarly, Chernov gives the experimental value of the hydrated surface energy as being roughly $10^{-3}\frac{J}{m^2}$. Mapping to the cubic lattice where there is one bond per unit cell area, this gives $\varepsilon \simeq 10^{-3}\frac{J}{m^2} \times 20$ nm$^2 = 2 \times 10^{-20}$ J, which in turn gives $k_BT/\varepsilon \simeq 0.25\frac{T}{300\ K}$. This number is only indicative, as the actual values depend strongly on factors such as the precipitants and salts used in the solution.

■ THE ACTIVE SOLUTION MODEL

To go beyond the standard SOS model and to include the effect of diffusive mass transport in the fluid, we consider a rectangular simulation cell consisting of a lattice of $N_x \times N_y \times N_z$ unit cells (see Figure 2). The lower part of the cell contains a standard SOS crystal: that is, fully filled columns of molecules as in the SOS model. Above the SOS crystal are solute molecules which are monomers that are free to move by random hops to any of their empty nearest-neighbor sites. The top of the simulation cell is open so that a molecule at position (i, j, N_z) that hops in the $+z$ direction will be lost to the simulation. To compensate, molecules randomly enter at the top of the simulation cell just as in the SOS model molecules randomly land on the surface. At the crystal surface, molecules can detach as in the SOS model and enter the solution but the random appearance of molecules in the SOS model is replaced by solute molecules attaching to the crystal. We now examine each of these steps in the simulations more carefully.

Movement in the Solution. At any given moment, the solution above the crystal will contain some number $N_{fluid}(t)$ of solute molecules. These move by making random jumps to nearest-neighbor sites. Each cell can only hold a single
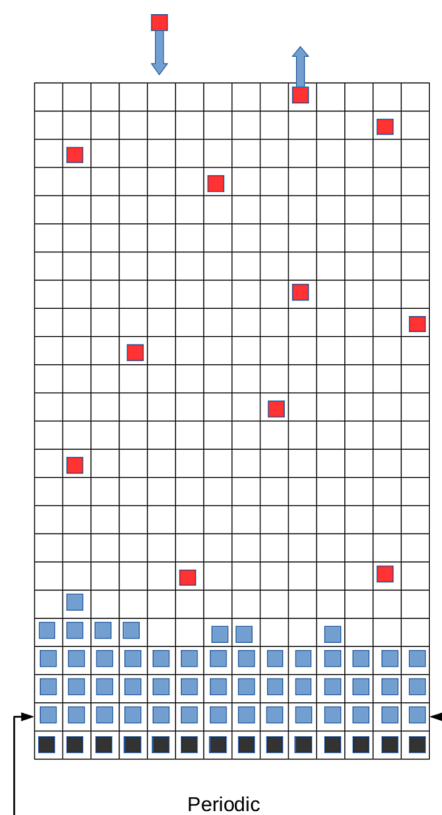
Figure 2. Two-dimensional version of our simulation cell. The blue squares are molecules that are bound to the crystal. The black squares are also crystal molecules but they are frozen and do not move. The red squares are molecules in solution. Molecules in solution move by jumping to nearest-neighbor sites, and the upper boundary of the simulation cell is open with particles free to leave. Molecules randomly enter at the top boundary. The other (horizontal) boundaries are periodic.

molecule so that jumps to occupied cells are prohibited. This excluded volume effect is the only interaction between molecules in solution: we take no account of intermolecular bonding in solution and so do not allow for the formation of oligomers.

Attachment and Detachment of Molecules. Consider the SOS crystal at $x-y$ position (i, j) and having height H_{ij}. This means that the lattice is filled with bound crystal molecules from position $(i, j, 1)$ until (i, j, H_{ij}) and that the first potentially empty cell is at $(i, j, H_{ij} + 1)$. The obvious method to handle molecular attachment to and detachment from the crystal is to imagine that whenever a solute molecule hops into this position it automatically binds to the crystal. However, this can lead to complicated behaviors in some circumstances. For example (see Figure 3), suppose that there is a solute molecule in the position $(i, j, H_{ij} + 2)$ and that one hops into the cell $(i, j, H_{ij} + 1)$ (say by a lateral hop from $(i, j - 1, H_{ij} + 1)$ as in Figure 3). Then if it automatically binds to the crystal, does that mean that the molecule at $H_{ij} + 2$ also binds at that moment? This is certainly possible, but in order to have an equilibrium state, it is necessary that the kMC algorithm respect microscopic detailed balance. This means that, for any possible move, the inverse must be possible. In the present case, we would have to allow molecules to leave the crystal not only from the upper most position of each column but also from any other position that is adjacent to an unoccupied cell.
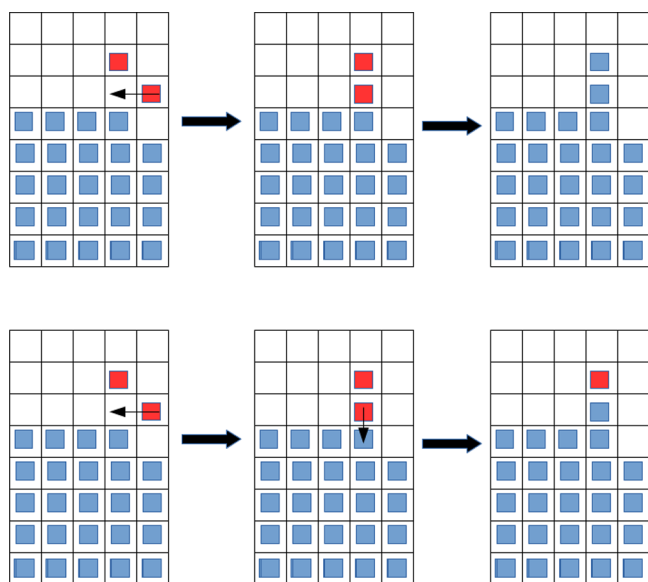
Figure 3. Illustration of the problems that arise if molecules automatically bind to the solid when they are in contact with it. The upper three frames show a molecule moving into an open space and forcing a neighbor molecule to bind to the solid as a consequence: detailed balance would require that the reverse move also occurs. The lower three frames show how binding occurs in our model: a molecule in contact with the solid does not bind to it until it tries to move in the $-z$ direction.

Analogous, but more complicated, possibilities are easy to imagine.

In keeping with the spirit of the original SOS model, we avoid these complications by using a different criterion for attachment (and detachment). In our model, a molecule at the position $(i, j, H_{ij} + 1)$ does not attach to the crystal. Instead, it only attaches when it tries a further move consisting of a hop *into* the crystal (that is, in the $-z$ direction). Similarly, if the surface molecule at (i, j, H_{ij}) is chosen for detachment, it does not move but only breaks its bond with the crystal (becoming a solute molecule). Only jumps in the $-z$ direction lead to attachment: a molecule that tries to jump from say $(i - 1, j, H_{ij} - 1)$ to $(i, j, H_{ij} - 1)$ when there is a molecule at that position does not attach to the crystal—the jump is simply blocked (excluded volume). Maintaining the privileged nature of the z direction is necessary to preserve the spirit of the SOS model.

Molecules Entering and Leaving at the Top of the Cell: Boundary Conditions. The stepped boundary conditions are still necessary to study crystal growth, and this presents complications at the top of the simulation cell. Normally, a molecule leaves the simulation cell if it is at position (i, j, N_z) and tries to jump in the $+z$ direction. Similarly, molecules enter the simulation by randomly appearing at positions (i, j, N_z). However, with stepped periodic boundaries, a solute molecule at the position (N_x, j, N_z) that hops in the $+x$ direction ends up at the position $(0, j, N_z + 1)$, which means that it also leaves the simulation volume. In order to preserve a detailed balance, it is therefore necessary that the reverse move be possible: namely, that the rate at which molecules enter the simulation cell at the site (N_x, j, N_z) is double that of the sites $(i < N_x, j, N_z)$. Failure to respect this condition leads to irregularities in the density profiles near the upper boundary.

Algorithm. The kMC algorithm makes use of the following rates.

- $r_{jump}(l; \hat{\mathbf{e}}_\alpha) = \nu_{jump}\chi(l; \hat{\mathbf{e}}_\alpha)$: the rate of jumps of a solute molecule l in the direction $\hat{\mathbf{e}}_\alpha$. $\chi(l; \hat{\mathbf{e}}_\alpha)$ is 1 if the target site is unoccupied and zero otherwise.
- $r_{add}(i, j, N_z) = \nu_{add}e^{\beta\mu}(1 + \delta_{iN_x})$: the rate at which molecules enter at the top of the cell from the uniform fluid, with chemical potential μ, above it.
- $r_{detach}(i, j, H_{ij}) = \nu_{detach}e^{\beta E_{ij}}$: the rate at which molecules detach from the surface position at $x = i$ and $y = j$.

The quantities ν_{jump}, ν_{add}, and ν_{detach} have the units of inverse time and are called the attempt frequencies. We also choose a frequency ν_0 which satisfies

$$\max\left(\frac{r_{jump}}{\nu_0}, \frac{r_{add}}{\nu_0}, \frac{r_{detach}}{\nu_0}\right) \leq 1 \tag{1}$$

where the maximum is taken over all possible configurations of the system. This can be simplified using $\max(r_{jump}) = \nu_{jump}$ and $\max(r_{ij}^+) = 2\nu_{add}e^{\beta\mu}$. For the rate of detachment, we note that, in the present case, where all bonds have the same energy, the maximum energy of a bound molecule occurs for the case of an admolecule with a single bond so that $\max(r_{detach}) = \nu_{detach}e^{-\beta\varepsilon}$ and so

$$\max\left(\frac{\nu_{jump}}{\nu_0}, \frac{\nu_{add}e^{\beta\mu}}{\nu_0}, \frac{\nu_{detach}e^{-\beta\varepsilon}}{\nu_0}\right) \leq 1 \tag{2}$$

Since all quantities are positive, the best choice in the present case is $\nu_0 = \max(\nu_{jump}, \nu_{add}e^{\beta\mu}, \nu_{detach}e^{-\beta\varepsilon})$. With the value of ν_0 fixed, the algorithm is as follows:

- Determine the number $\mathcal{N}_t$ of elementary events. These are molecules entering the cell ($(N_x + 1) \times N_y$ possibilities for the "twist" boundary conditions), fluid molecules jumping ($6N_{Fluid}(t)$ possibilities), and molecules detaching from the surface ($N_x \times N_y$ possibilities), giving a total of $\mathcal{N}_t = 2N_xN_y + N_y + 6N_{Fluid}(t)$.
- Choose one, call it $\mathcal{E}$, of the $\mathcal{N}(t)$ possible events and let the rate associated with it be $r(\mathcal{E})$.
- Execute the event with the probability $r(\mathcal{E})/\nu_0$.
- Advance the time by $\delta t = \frac{1}{\nu_0\mathcal{N}_t}$.
- Has the stopping criterion been achieved? If yes, end, and if no, go to step 1.

We confirm that the rate at which any particular event $\mathcal{E}$ occurs is in fact $\frac{1}{\mathcal{N}_t} \times \frac{r(\mathcal{E})}{\nu_0} \times \frac{1}{\delta t} = r(\mathcal{E})$, as it should be.

Finally, it is worth noting that the only quantities with the units of time are the attempt frequencies and the derived quantities of the scale factor ν_0 and the time step. It is enough to express all times in terms of any one of the frequencies ν_x so that the dimensionless time step is $\delta t^* = \nu_x\delta t$ and the dimensionless frequencies are $\nu_{jump}^* = \nu_{jump}/\nu_x$ etc., in which case the only independent parameters are the dimensionless ratios ν_{detach}/ν_{jump} and ν_{add}/ν_{jump}.

Equilibrium. *Solute Concentration.* In equilibrium the concentration of solute molecules will be, on average, uniform (call it c_{eq}) and so their total number will be constant. The rates at which molecules enter and leave must balance in equilibrium. The rate at which molecules leave the cell will be the total number in the topmost layer, $c_{eq}a^3N_xN_y$ times the probability of a jump in the $+z$ direction. The number at which

they enter will be determined by the stochastic insertion of particles so that

$$c_{eq} a^3 N_x N_y \times \nu_{jump}$$
$$= \sum_{i=1}^{N_x} \sum_{j=1}^{N_y} r_{add}(i, j, N_z) \times p_{unoccupied}(i, j, N_z) \tag{3}$$

where $p_{unoccupied}(i, j, N_z) = (1 - c_{eq} a^3)$ is the probability that a given cell is empty. Thus

$$a^3 c_{eq} N_x N_y \nu_{jump} = \nu_{add} e^{\beta \mu} (N_x N_y - c_{eq} a^3 N_x N_y) \tag{4}$$

from which

$$\frac{a^3 c_{eq}}{1 - a^3 c_{eq}} \nu_{jump} = \nu_{add} e^{\beta \mu} \tag{5}$$

This can be viewed as giving the equilibrium concentration as a function of the rates or as determining one of the rates, e.g. ν_{add}, as a function of the desired concentration.

Solute Diffusion Constant. The solute molecules make random jumps to nearest-neighbor sites with the rate $r_{jump}(l; \hat{\mathbf{e}}_\alpha)$. Let $\mathbf{s} = (i, j, k)$ be some lattice site in the region of the bulk fluid (away from the open boundary at the top and the crystal surface at the bottom). The excluded volume effect means that at any time t the number of solute molecules at that site, $n_t(\mathbf{s})$, is either 0 or 1 and so the average number, $\langle n_t(\mathbf{s}) \rangle$, lies between these values. At low concentrations, for which excluded volume effects can be ignored, it evolves as

$$\langle n_{t+\delta t}(\mathbf{s}) \rangle = \langle n_t(\mathbf{s}) \rangle + \sum_{\alpha=1}^{6} \frac{1}{\mathcal{N}_t} \frac{\nu_{jump}}{\nu_0} \langle n_t(\mathbf{s} + \hat{\mathbf{e}}_\alpha) \rangle$$
$$- \sum_{\alpha=1}^{6} \frac{1}{\mathcal{N}_t} \frac{\nu_{jump}}{\nu_0} \langle n_t(\mathbf{s}) \rangle \tag{6}$$

where the second term on the right is the probability that in one time step, a molecule jumps from a nearest neighbor site into the site $\mathbf{s}$ and the last term is the probability that a molecule jumps from the site $\mathbf{s}$ to a neighboring site. Rearranging gives

$$\frac{\langle n_{t+\delta t}(\mathbf{s}) \rangle - \langle n_t(\mathbf{s}) \rangle}{\delta t} = \frac{1}{\mathcal{N}_t} \frac{a^2 \nu_{jump}}{\delta t \nu_0}$$
$$\sum_{\alpha=1}^{3} \frac{\langle n_t(\mathbf{s} + \hat{\mathbf{e}}_\alpha) \rangle + \langle n_t(\mathbf{s} - \hat{\mathbf{e}}_\alpha) \rangle - 2\langle n_t(\mathbf{s}) \rangle}{a^2} \tag{7}$$

or, in the continuum limit, the diffusion equation

$$\frac{\partial}{\partial t} \langle n_t(\mathbf{s}) \rangle = D \nabla^2 \langle n_t(\mathbf{s}) \rangle \tag{8}$$

with diffusion coefficient

$$D = \frac{a^2 \nu_{jump}}{\delta t \nu_0 \mathcal{N}_t} = a^2 \nu_{jump} \tag{9}$$

Surface: Relation to SOS Model. For a surface in equilibrium (i.e., at coexistence with the solution), the rate at which molecules attach is

$$r_{attach} = c_{eq} N_x N_y \nu_{jump} \tag{10}$$

To establish a connection with the SOS model, recall that in it molecules attach to the surface stochastically at a rate

$$r_{attach}^{SOS} = N_x N_y \nu_{add}^{SOS} e^{\beta \mu^{SOS}} \tag{11}$$

Equating these two expressions for an equilibrium system—for which the crystal and the solution coexist—gives

$$N_x N_y \nu_{add}^{SOS} e^{\beta \mu^{SOS}} = c_{eq} N_x N_y \nu_{jump} = (1 - c_{eq}) N_x N_y \nu_{add} e^{\beta \mu^{coex}} \tag{12}$$

so

$$e^{\beta \mu^{SOS}} = (1 - c_{eq}) \frac{\nu_{add}}{\nu_{add}^{SOS}} e^{\beta \mu^{coex}} \tag{13}$$

which suggests that we should take $\nu_{add} = \nu_{add}^{SOS}/(1 - c_{eq})$ so that the chemical potential has the same meaning as in the SOS model. Since c_{eq} is generally small in our work, it is sufficient to take $\nu_{add} = \nu_{add}^{SOS}$.

Mapping to Real Units. In order to translate the simulation result into real units, one needs to determine the units of time, distance, and mass. In the simulations, all times t are given in terms of the dimensionless parameter $\nu_{detach} t$ so that what is really needed is the physical value of the attempt frequency. In the fluid phase, the molecules move diffusively with a diffusion constant equal to $D = \nu_{jump} a^2$ with the dimensionless ratio $p_{jump} = \nu_{jump}/\nu_{detach}$ being an input parameter. The lattice spacing a is the typical size of the molecules; thus, given the tracer-diffusion constant of the molecules in solution, the attempt frequency is determined as $\nu_{detach} = D/a^2 p_{jump}$. For the energy scale, we can estimate the surface tension at low temperatures as approximately $\gamma = \varepsilon/2a^2$ and match to experimental values from crystallization experiments. Using some typical data for lysozyme of $a \approx 4$ nm, $\gamma \approx 1$ mJ/m^2, and $D \approx 10^{-6}$ cm^2/s gives $\nu_{detach} = \frac{6.25 \times 10^6}{p_{jump}} s^{-1}$. A typical value of lysozyme concentration at coexistence is on the order of 10 mg/mL, which given the atomic weight of the protein as 14.4×10^3 u corresponds to a number density of $n = 4 \times 10^{-3}$ nm^{-3} or $na^3 = 0.026$.

■ CRYSTAL GROWTH UNDER QUIESCENT CONDITIONS

Parameters. Before beginning a discussion of various effects, we pause to summarize the parameters that go into the simulations. There are three dimensionful parameters: the bond strength ε, the lattice spacing a, and the detachment frequency ν_{detach}, which are generally only needed in making a comparison to experimental data. We express all other quantities in dimensionless units wherein energies are scaled to ε, times to ν_{detach}, and lengths to a. Dimensionless quantities will be denoted by an asterisk.

The remaining, dimensionless, parameters are

- Geometric: N_x, N_y and N_z
- Thermodynamic:
    - Temperature, $T^* \equiv k_B T/\varepsilon$
    - Applied supersaturation, $\Delta \mu^* \equiv (\mu - \mu_{eq})/\varepsilon$
- Kinetic:
    - Addition frequency, ν_{add}^*
    - Jump frequency, ν_{jump}^*

Important derived quantities are

- The equilibrium concentration for a given chemical potential, $\frac{c_{eq}*}{1 - c_{eq}*}\nu_{jump}* = \nu_{add}*e^{\beta\mu} \leftrightarrow c_{eq}* \frac{\nu_{add}* e^{\beta\mu}}{\nu_{jump}* + \nu_{add}* e^{\beta\mu}}$. (Note that the low density limit $c_{eq}* \simeq \frac{\nu_{add}*}{\nu_{jump}*}e^{\beta\mu}$ is usually a good approximation.) In general, including nonequilibrium situations such as during crystal growth, $c_{eq}*$ can be thought of as the concentration in the well-stirred reservoir above the open boundary.

- The equilibrium—i.e. coexistence—concentration for a step, $\nu_{jump}* c_{coex}* = e^{-3\beta\varepsilon}$. From the previous identification of the relation between applied chemical potential and solute density, this implies that $\frac{\nu_{jump}* \nu_{add}*}{\nu_{jump}* + \nu_{add}* e^{\beta\mu}} e^{\beta\mu_{coex}} = e^{-3\beta\varepsilon}$.

- The diffusion constant $D* = \nu_{jump}*$.

Physically, $\nu_{jump}*$ determines the diffusion constant and $\nu_{add}*$ determines the solubility at coexistence. Note that in general the ratio of the bulk concentration to that at coexistence is

$$\frac{c_{eq}*}{c_{coex}*} = \frac{e^{\beta\mu}}{e^{\beta\mu_{coex}}} = e^{\beta(\mu - \mu_{coex})} \equiv e^{\beta\Delta\mu} \tag{14}$$

and so we will use the term "supersaturation" interchangeably for both $c_{eq}*/c_{coex}*$ and for $\Delta\mu*$ with the appropriate quantity being clear from the context.

Density Profile in the Fluid. When a step grows, it consumes solute molecules and therefore depletes the solution above the crystal. This is illustrated in Figure 4, which shows
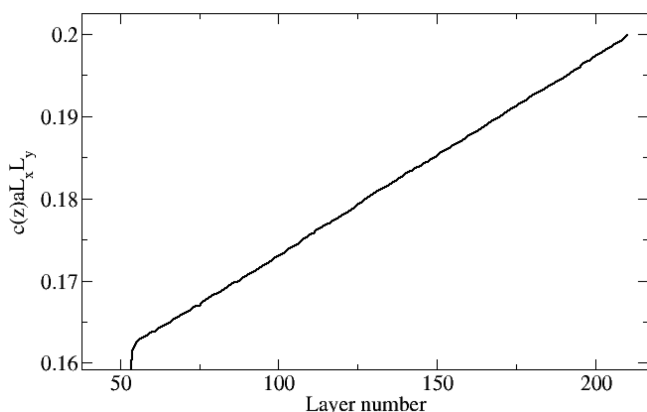
Figure 4. Average number of solute molecules in each x–y plane from a simulation with applied chemical potential $\Delta\mu = 0.2$ at temperature $k_BT = 0.25\varepsilon$ and with $p_{jump} = 1$. The figure illustrates the highly linear profile resulting from the interaction of step growth and diffusion. Note that the crystal height, which is the lower limit of the volume available to the fluid, is about 50 layers.

the average number of solute molecules in each x–y plane as a function of z. Assuming that diffusion is fast relative to the rate of step growth, one can average over the x–y planes to get the average concentration as a function of z, $c(z; t)$, which then satisfies the one-dimensional diffusion equation

$$\frac{\partial c(z; t)}{\partial t} = D\frac{\partial^2}{\partial z^2}c(z; t) \tag{15}$$

A simple analysis of the kinetics (see the Supporting Information) gives to lowest order

$$c(z; H_t) = c_0 + (c_{eq} - c_0)\frac{z - H_t}{L_z - H_t}$$

$$v(c_0; H_t) = a^2 D(c_{eq} - c_0)\frac{L_x}{H_t - L_z} \tag{16}$$

where H_t is the height of the crystal at time t and $v(c)$ is the step velocity when the concentration at the surface is c. The figure shows that this linear prediction is confirmed.

The solute concentration at the crystal surface, c_0, is determined by a balance between the rate of consumption of solute molecules by step growth and the rate at which new molecules arrive at the surface due to diffusion. The former increases with increasing concentration at the surface: the higher the (local) supersaturation, the faster the step growth. The latter decreases with increasing concentration at the surface: the less the difference between the concentration at the surface and the concentration at the boundary, $c(L_z)$, the lower the concentration gradient and the lower, in turn, the diffusional flux. Thus, if at one extreme $c_0 = c(L_z)$, then step growth will be fast but the diffusional current will be zero. At the other extreme, if $c_0 = c_{eq}$, then step growth will be zero but the diffusional current will be high. Figure 5 shows the measured step velocity as a function of the applied supersaturation and the measured effective supersaturation at the crystal surface for different values of the system size, L_z, at a temperature of $k_BT/\varepsilon = 0.25$. (The effective supersaturation is determined by averaging the number of molecules in the layer directly above the crystal surface during the simulation—the quantity c_0—and then defining $\Delta\mu_{eff} = k_BT \ln\frac{c_0}{c_{eq}} \simeq k_BT\frac{c - c_{eq}}{c_{eq}}$.) It is clear that the size dependence is rather weak in terms of the step velocity as a function of $\Delta\mu$ and that it disappears entirely when the step velocity is considered as a function of supersaturation at the surface. Fitting the data to a quadratic gives

$$v(c) = v_1\left(\frac{c - c_{eq}}{c_{eq}}\right) + v_2\left(\frac{c - c_{eq}}{c_{eq}}\right)^2 \text{ with } v_1 = 9.34 \times 10^{-7}a\nu_{detach}$$

and $v_2 = 2.31 \times 10^{-7}a\nu_{detach}$ over a range $0 < \frac{c - c_{eq}}{c_{eq}} < 1.05$.

Using this fit in eq 16 gives a quadratic equation for the concentration at the surface which can be written as

$$v_2\left(\frac{c_0 - c_{eq}}{c_{eq}}\right)^2 + \left(v_1 + a^2 D\frac{c_{eq}}{L_z - H}L_x\right)\left(\frac{c_0 - c_{eq}}{c_{eq}}\right)$$

$$= a^2 D\frac{c(L_z) - c_0}{L_z - H}L_x \tag{17}$$

Figure 6 shows that this expression gives values of the effective supersaturation at the crystal surface that are in good agreement with those obtained from simulation.

Constant Effective Supersaturation. As the crystal grows, the distance between its surface and the open boundary decreases, leading to a change in the effective supersaturation. The effect is not large but is nevertheless noticeable, as illustrated in Figure 7. This can be almost entirely eliminated by reconsidering the mass balance between the processes of diffusion and crystal growth. As discussed in the Supporting Information, the total rate of change of mass of the crystal can be expressed as
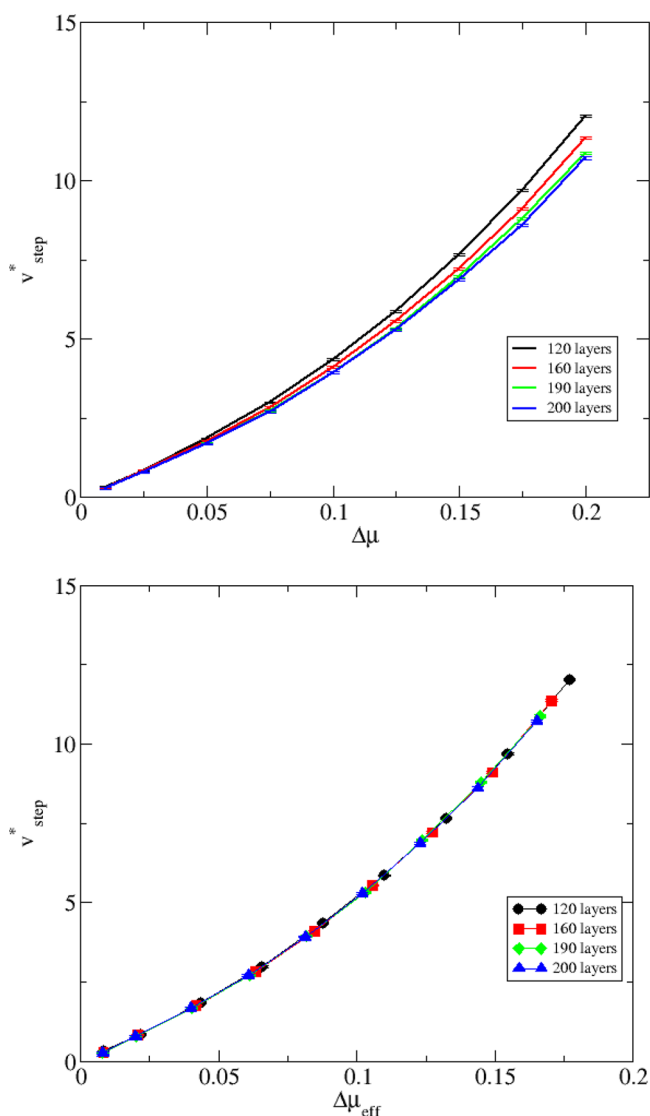
Figure 5. Step velocity versus applied supersaturation (top panel) and effective supersaturation at the crystal surface (bottom panel) for different numbers of layers in the bulk fluid. While the top panel shows a dependence of step velocity on system height, the bottom panel shows that this is entirely accounted for by the difference in effective supersaturation. The dimensionless step velocity is defined as $v^* = v/v_0$, where $v_0 \equiv 10^7 a^2 v_{\text{detach}}$. The effective supersaturation at the surface is calculated as $\beta\Delta\mu = \ln(c_0/c_{\text{coex}})$.

$$\frac{d\text{M}}{dt} = \frac{L_y v}{a^2} = -D\left(\frac{\partial c_t(z)}{\partial z}\right)_{H_t} L_x L_y \tag{18}$$

and substituting the approximate linear profile and rearranging gives

$$c(L_z) = c_0 + \frac{1}{D}\frac{L_z - H(t)}{L_x L_y}\frac{d\text{M}}{dt} \tag{19}$$

With a fixed value of concentration at the open boundary, this relation implies that the concentration at the surface is a function of time. If on the other hand, we wish to keep c_0 constant, then $c(L_z)$ must depend on time. Subtracting the relation at time 0 from that at time t gives
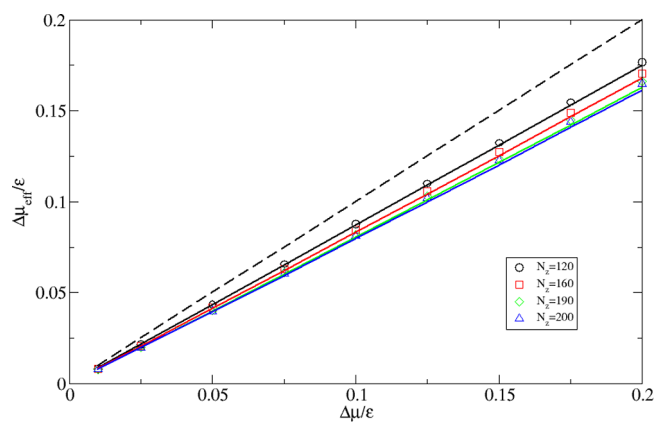
Figure 6. Effective excess chemical potential at the crystal surface versus the applied supersaturation at the open boundary. The effective excess is determined by averaging the concentration in the cells just above the crystal surface. The dashed line corresponds to $\Delta\mu_{\text{eff}} = \Delta\mu$, and the symbols are from simulations with different values of N_z. The lines are determined from eq 17 and show that the theory gives a good account of the dependence of the effective supersaturation on the parameters.
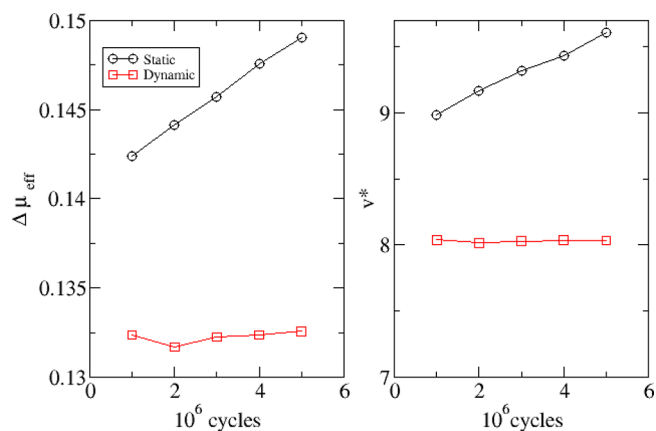
Figure 7. (left) Supersaturation at the crystal surface as a function of time for the static and dynamic open boundary. Each point is an average over 10^6 cycles. (right) Corresponding step velocities. The dynamic scheme eliminates most of the variation of the effective supersaturation due to crystal growth.

$$c_t(L_z) - c_{t=0}(L_z) = \frac{1}{D}\frac{H(0) - H(t)}{L_x L_y}\frac{d\text{M}}{dt} \tag{20}$$

where we now assume that because c_0 is constant, so is $d\text{M}/dt$. In that case, it follows that $d\text{M}/dt = (M(t) - M(0))/t = L_x L_y(H(t) - H(0))/t$, giving the final relation

$$c_t(L_z) = c_{t=0}(L_z) - \frac{(M(t) - M(0))^2}{D(L_x L_y)^2 t} \tag{21}$$

This is implemented by using eq 16 to extract the time-varying value of r_{add} and using this in the simulations. The effectiveness of this scheme is illustrated in Figure 7, where the supersaturation at the crystal surface and the step velocities are shown for simulations with and without this condition.

■ THE EFFECT OF FLOW

To illustrate the interaction between crystal growth and transport in the fluid phase, we use it to study the effect of flow

on crystal growth. Flow is easily incorporated into our model by biasing the probabilities to jump forward and backward in each direction: in principle, these biases can depend on position to simulate an inhomogeneous flow field. In the following, our goal is to illustrate the model and to indicate some of the difference that flow can cause relative to the standard SOS model and so we use the simplest example of a uniform flow field. This ignores such important physical effects as the formation of a boundary layer at the crystal surface and so cannot be expected to correspond to any real experiment. However, we note that for the systems we have in mind, e.g. large biological molecules in water, the nature and effect of a boundary layer for the flow will in any case be complicated for several reasons. Most importantly, in the case of the water molecules are some 10−100 times smaller than the crystal-forming species and so the interaction with the crystal surface will be highly nontrivial and consequently the nature of the boundary layer, the slip length, its dependence from the edge of a finite crystal, etc. may be hard to predict. As our goal here is to illustrate our model, we therefore ignore these complications and simply address the following question: if a flow is present near the crystal surface, what effect will it have on step growth? We therefore replace the equal probability, $\frac{\nu_{jump}}{\nu_0}$, to hop in, say, the $\hat{\mathbf{x}}$ and $-\hat{\mathbf{x}}$ directions, by a biased jump with relative probabilities $(1 + q)\frac{\nu_{jump}}{\nu_0}$ and $(1 - q)\frac{\nu_{jump}}{\nu_0}$ respectively, where $0 \leq q \leq 1$. If the probabilities for jumps in the other directions remain unchanged, this causes the macroscopic diffusion equation (eq 6) to be generalized to

$$\langle n_{t+\delta t}(\mathbf{s}) \rangle = \langle n_t(\mathbf{s}) \rangle + \frac{1}{\mathcal{N}_t}\frac{\nu_{jump}}{\nu_0}\sum_{\hat{\mathbf{e}}=\hat{\mathbf{y}},\hat{\mathbf{z}}}(\langle n_t(\mathbf{s} + \hat{\mathbf{e}})\rangle$$
$$+ \langle n_t(\mathbf{s} - \hat{\mathbf{e}})\rangle - 2\langle n_t(\mathbf{s} + \hat{\mathbf{e}})\rangle)$$
$$+ \frac{1}{\mathcal{N}_t}\frac{\nu_{jump}}{\nu_0}((1 + q)\langle n_t(\mathbf{s} + \hat{\mathbf{x}})\rangle$$
$$+ (1 - q)\langle n_t(\mathbf{s} - \hat{\mathbf{x}})\rangle - 2\langle n_t(\mathbf{s} + \hat{\mathbf{x}})\rangle) \tag{22}$$

or

$$\langle n_{t+\delta t}(\mathbf{s}) \rangle = \langle n_t(\mathbf{s}) \rangle + \frac{1}{\mathcal{N}_t}\frac{\nu_{jump}}{\nu_0}\sum_{\hat{\mathbf{e}}=\hat{\mathbf{x}},\hat{\mathbf{y}},\hat{\mathbf{z}}}(\langle n_t(\mathbf{s} + \hat{\mathbf{e}})\rangle$$
$$+ \langle n_t(\mathbf{s} - \hat{\mathbf{e}})\rangle - 2\langle n_t(\mathbf{s} + \hat{\mathbf{e}})\rangle)$$
$$+ \frac{1}{\mathcal{N}_t}\frac{\nu_{jump}}{\nu_0}q(\langle n_t(\mathbf{s} + \hat{\mathbf{x}})\rangle - \langle n_t(\mathbf{s} - \hat{\mathbf{x}})\rangle) \tag{23}$$

which, in the continuum limit becomes the advection−diffusion equation

$$\frac{\partial}{\partial t^*}\langle n_t(\mathbf{s})\rangle = c^*\frac{d}{dx^*}\langle n_t(\mathbf{s})\rangle + D^*\nabla^{*2}\langle n_t(\mathbf{s})\rangle \tag{24}$$

with advection velocity

$$c^* = \frac{1}{a\nu_{detach}} \times \frac{a\nu_{jump}}{\delta t\nu_0\mathcal{N}_t}q = p_{jump}q \tag{25}$$

We can get an idea of the scale of this flow using our previous estimates for lysozyme:

$$c = p_{jump}qa\nu_{detach} = q \times 2.5 \text{ cm/s} \tag{26}$$

Larger velocities are possible but would require a smaller time step.

Flow Perpendicular to the Step Front. Our first results are for flow perpendicular to the direction of step growth: that is, flow into or away from the step face. Figure 8 shows the step
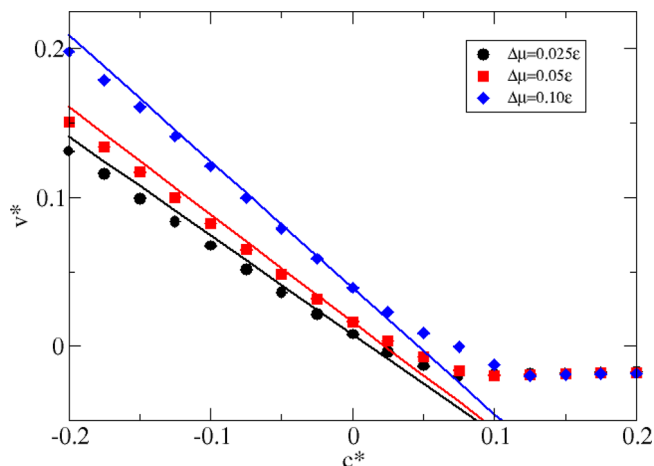
Figure 8. Step velocity, $v^* = 10^7 \times v/(a\nu_{detach})$, as a function of the dimensionless flow velocity c^* for flows perpendicular to the step front and for three values of supersaturation. The lines are predictions of the simple analytic model (eq 27). The simulations were performed using $T^* = 0.25$ and $p_{jump} = 1$.

velocity as a function of the flow velocity (the parameter q above) for three different supersaturations. For negative velocities, which means flows into the step, increasing flow velocity leads to increasing step velocity due to the increased rate at which material is delivered to the step. Similarly, for positive flow velocities, meaning flows away from the step, less material arrives at the step front and so growth slows. In fact, for sufficiently high velocities, no material reaches the step front and the step dissolves. Most of the dependence of step velocity on flow velocity can be explained by simply assuming that all of the material advected to the step front gets incorporated into the step so that the step velocity becomes
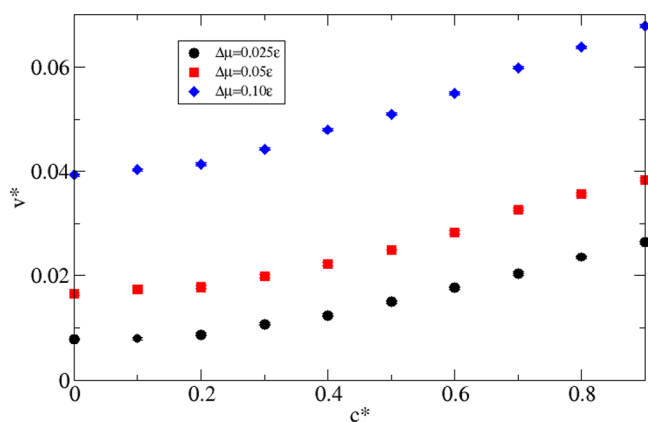
$$v = v^*\left(\frac{c_0 - c_{eq}}{c_{eq}}\right) + p_{jump}q \times a^3c_0 \tag{27}$$

This also works for small positive velocities until so much material is advected away from the step that the local concentration of solute at the step front drops to zero and the rate of step dissolution is entirely determined by the rate of detachment: it is then not affected by further increases in flow velocity (nor does it depend on the supersaturation).

Flow Parallel to the Step Front. More surprisingly, flow parallel to the step front also affects the growth rate. Figure 9 shows the step velocity as a function of flow velocity for parallel flows and three supersaturations. The effect is much weaker than for perpendicular flows since it can only act on fluctuations in the step front and, particularly, on kink sites.
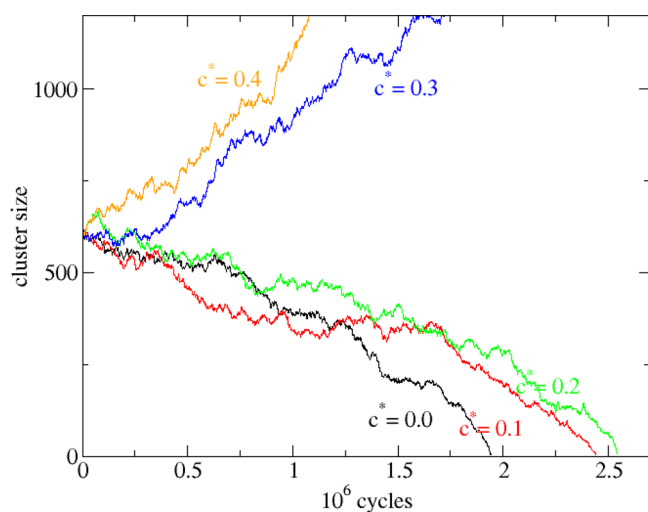
Islands. New effects are seen when the growth of 2D islands rather than planar step fronts is considered. For the idealized case of circular islands, any uniform flow will have perpendicular components into the island for half of its circumference and away from the island for the other half. We therefore expect that islands will grow asymmetrically in flow and, particularly on the basis of Figure 8, that the enhancement

Figure 9. As for Figure 8 but for flows parallel to the step face.

Figure 11. Change in critical cluster size as a function of the flow velocity. For supersaturations of $\Delta\mu = 0.025\varepsilon$ (left panel) and $\Delta\mu = 0.05\varepsilon$ (right panel) six simulations were performed at different flow velocities c^*, beginning with clusters of various radii (expressed in lattice constants). The simulations were terminated when the clusters either doubled in size or dissolved completely (size 0). The average final size over the six runs is shown by the colors as indicated: red therefore means unambiguously supercritical, and blue is unambiguously subcritical. The diminution in critical radii as a function of flow velocity is evident.
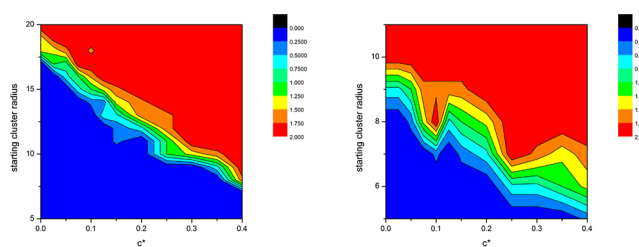
of growth in the former will be more important than that of dissolution in the latter. This is confirmed in Figure 10,

Figure 10. Rate of change of cluster mass of individual 2-D islands under different flow conditions at $\Delta\mu = 0.025\varepsilon$ and for different flow velocities, demonstrating that increasing the flow velocity can result in subcritical islands becoming supercritical.

showing the rate of change of the total mass of a cluster as a function of time for different flow rates. With no flow, the cluster is subcritical and thus evaporates. As the flow velocity increases, the rate of evaporation becomes slower until, for sufficiently high flows, the cluster grows. We have therefore investigated the effect of flow on the critical radii of clusters. For the given simulation conditions, we began with clusters of a given radius and allowed them to evolve until they either evaporated or doubled in size. The latter was taken to be an indication that they are supercritical. This was done six times and the number of times the cluster doubled in size was recorded (see Figure 11). Under the quiescent condition, the observed critical radii (between 17 and 18 lattice units for $\Delta\mu = 0.025$ and between 9 and 10 for $\Delta\mu = 0.05$) agree well with previous, more extensive determinations.[24] With flow, one sees a roughly linear decrease in critical radius as a function of flow velocity.

The asymmetric effect of flows on clusters can lead to another interesting effect which is cluster drift (see Figure 12 and movies 1 and 2 in the Supporting Information). When it is subjected to a flow, half of the cluster will experience growth-

inducing flow while the other half will experience evaporation-inducing flow. Thus in general, one side will grow faster than the other and the center of mass of the cluster will drift upwind of the flow. For near-critical clusters, it is possible that the evaporation-inducing flow will lead to actual evaporation of the trailing edge of the cluster at the same time as the leading edge gains mass so that the overall change in mass as the cluster moves will be slow or even close to zero. In this case, clusters appear to move spontaneously against the flow.

■ CONCLUSIONS

In this paper we have described a new kinetic Monte Carlo simulation algorithm for step growth that includes a representation of the molecules in solution undergoing diffusive motion. The algorithm represents a hybrid of the usual solid-on-solid model and kMC model of the solution. As such, it goes beyond the "instantaneous" kinetics of the SOS model and allows the introduction of flows, the study of competition for material, and other effects. We noted that care must be taken to distinguish between the supersaturation at the crystal surface and that applied at the top of the simulation cell.

We have used our model to study the effect of flows on step growth and on island evolution. The flows we have studied are artificial ones in which molecules move at a constant velocity in the fluid, independent of their position and unaffected by the crystal surface. Realistic flows will be more complex, involving boundary layers and position-dependent velocity fields. Rather than modeling such realistic flows, our goal was simply to look at the effect a steady flow could have if one were present. Flows perpendicular to step growth have the expected effect: flows into the step transport material enhance the step growth rate while flows away from the step remove material and can arrest step growth entirely and even reverse the processes into dissolution of the crystal. More surprisingly, we found that flows parallel to the step can also affect step growth rates. In this case, the effect is again due to enhanced transport of material by the flow but the interaction with the step is weaker, only enhancing the lateral growth at kink sites and other fluctuations away from a flat step. Finally, we showed that islands on a flat crystal surface are also strongly affected by flows with the critical radius for island formation being reduced as flow velocities are increased. Since any steady flows affect islands asymmetrically—transporting material toward half the
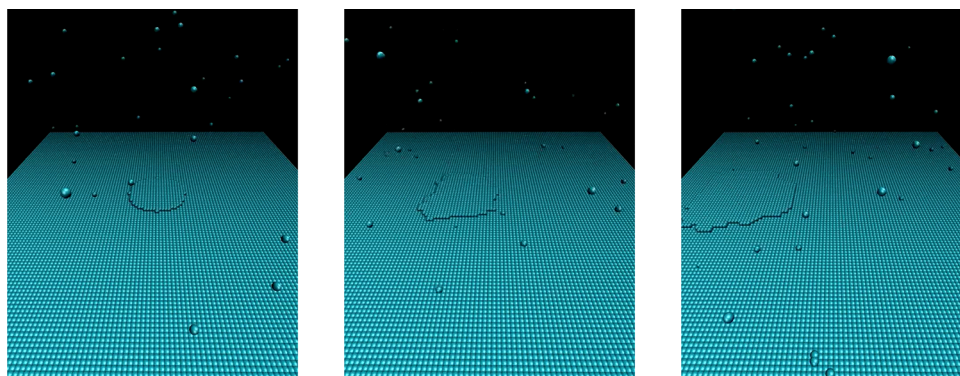
Figure 12. Evolution of an island in the presence of flow: the flow is from left to right in the figure. The leading half of the island grows while the trailing half dissolves, leading to a continuous motion of the center of mass in the direction opposite of the flow.

island and away from the other half—some islands move spontaneously in the direction opposite the flow. It is an intriguing question whether such flow-induced cooperative diffusion could be observed in experiments.

In conclusion, we believe that our model opens the possibility to perform more realistic studies of crystal growth taking into account the coupled nature of growth and transport in the fluid. This could prove particularly important to systems that involve a competition for material, such as macrosteps.

ASSOCIATED CONTENT

Supporting Information

The Supporting Information is available free of charge at https://pubs.acs.org/doi/10.1021/acs.cgd.9b01434.

> Multiscale analysis of crystal growth rate and a list of mathematical symbols and their definitions (PDF)
>
> Evolution of a two-dimensional island in the absence of flow (MP4)
>
> Evolution of a two-dimensional island in the presence of flow (MP4)

AUTHOR INFORMATION

Corresponding Author

James F. Lutsko — *Center for Nonlinear Phenomena and Complex Systems, Code Postal 231, Université Libre de Bruxelles, 1050 Brussels, Belgium;* orcid.org/0000-0001-9899-8435; Email: jlutsko@ulb.ac.be

Author

Dominique Maes — *Structural Biology Brussels, Vrije Universiteit Brussel, 1050 Brussels, Belgium;* orcid.org/0000-0002-9179-3186

Complete contact information is available at:
https://pubs.acs.org/10.1021/acs.cgd.9b01434

Notes

The authors declare no competing financial interest.

ACKNOWLEDGMENTS

REFERENCES

(1) Tsuchida, A.; Takyo, E.; Taguchi, K.; Okubo, T. Kinetic analyses of colloidal crystallization in shear flow. *Colloid Polym. Sci.* **2004**, *282*, 1105−1110.

(2) Penkova, A.; Pan, W.; Hodjaoglu, F.; Vekilov, P. G. Nucleation of Protein Crystals under the Influence of Solution Shear Flow. *Ann. N. Y. Acad. Sci.* **2006**, *1077*, 214−231.

(3) Forsyth, C.; Mulheran, P. A.; Forsyth, C.; Haw, M. D.; Burns, I. S.; Sefcik, J. Influence of Controlled Fluid Shear on Nucleation Rates in Glycine Aqueous Solutions. *Cryst. Growth Des.* **2015**, *15*, 94−102.

(4) Mura, F.; Zaccone, A. Effects of shear flow on phase nucleation and crystallization. *Phys. Rev. E: Stat. Phys., Plasmas, Fluids, Relat. Interdisc. Top.* **2016**, *93*, 042803.

(5) McPherson, A.; Malkin, A. J.; Kuznetsov, Y. G. Atomic Force Microscopy in the Study of Macromolecular Crystal Growth. *Annu. Rev. Biophys. Biomol. Struct.* **2000**, *29*, 361−410.

(6) Yau, S.-T.; Petsev, D. N.; Thomas, B. R.; Vekilov, P. G. Molecular-level thermodynamic and kinetic parameters for the self-assembly of apoferritin molecules into crystals. *J. Mol. Biol.* **2000**, *303*, 667−678.

(7) Sleutel, M.; Vanhee, C.; Van de Weerdt, C.; Decanniere, K.; Maes, D.; Wyns, L.; Willaert, R. The Role of Surface Diffusion in the Growth Mechanism of Triosephosphate Isomerase Crystals. *Cryst. Growth Des.* **2008**, *8*, 1173−1180.

(8) Sazaki, G.; Driessche, A. E. V.; Dai, G.; Okada, M.; Matsui, T.; Otalora, F.; Tsukamoto, K.; Nakajima, K. In Situ Observation of Elementary Growth Processes of Protein Crystals by Advanced Optical Microscopy. *Protein Pept. Lett.* **2012**, *19*, 743−760.

(9) Sleutel, M.; Willaert, R.; Gillespie, C.; Evrard, C.; Wyns, L.; Maes, D. Kinetics and Thermodynamics of Glucose Isomerase Crystallization. *Cryst. Growth Des.* **2009**, *9*, 497−504.

(10) Sleutel, M.; Maes, D.; Driessche, A. E. V. What can mesoscopic level in situ observations teach us about kinetics and thermodynamics of protein crystallization? *Adv. Chem. Phys.* **2012**, *151*, 223−276.

(11) Chernov, A. Notes on interface growth kinetics 50 years after Burton, Cabrera and Frank. *J. Cryst. Growth* **2004**, *264*, 499−518.

(12) Chernov, A. How does the flow within the boundary layer influence morphological stability of a vicinal face? *J. Cryst. Growth* **1992**, *118*, 333−347.

(13) Vekilov, P. G.; Thomas, B. R.; Rosenberger, F. Effects of Convective Solute and Impurity Transport in Protein Crystal Growth. *J. Phys. Chem. B* **1998**, *102*, 5208−5216.

(14) Vekilov, P.; Rosenberger, F. Protein crystal growth under forced solution flow: experimental setup and general response of lysozyme. *J. Cryst. Growth* **1998**, *186*, 251−261.

(15) Vekilov, P. G.; Rosenberger, F. Increased Stability in Crystal Growth Kinetics in Response to Bulk Transport Enhancement. *Phys. Rev. Lett.* **1998**, *80*, 2654−2656.

(16) Kadowaki, A.; Yoshizaki, I.; Adachi, S.; Komatsu, H.; Odawara, O.; Yoda, S. Effects of Forced Solution Flow on Protein-Crystal Quality and Growth Process. *Cryst. Growth Des.* **2006**, *6*, 2398−2403.

(17) Yu, Y.; Liu, Y.; Wang, X.; Oberthür, D.; Dierks, K.; Betzel, C. Effects of forced solution flow on lysozyme crystal growth. *Cryst. Res. Technol.* **2010**, *45*, 380−386.

(18) Ildefonso, M.; Candoni, N.; Veesler, S. A Cheap, Easy Microfluidic Crystallization Device Ensuring Universal Solvent Compatibility. *Org. Process Res. Dev.* **2012**, *16*, 556−560.

(19) Maruyama, M.; Kawahara, H.; Sazaki, G.; Maki, S.; Takahashi, Y.; Yoshikawa, H. Y.; Sugiyama, S.; Adachi, H.; Takano, K.; Matsumura, H.; Inoue, T.; Murakami, S.; Mori, Y. Effects of a Forced Solution Flow on the Step Advancement on 110 Faces of Tetragonal Lysozyme Crystals: Direct Visualization of Individual Steps under a Forced Solution Flow. *Cryst. Growth Des.* **2012**, *12*, 2856−2863.

(20) Sazaki, G.; Dai, G. Direct observation of bunching of elementary steps on protein crystals under forced flow conditions. *Theor. Appl. Mech. Lett.* **2015**, *5*, 173−176.

(21) Derby, J. The synergy of modeling and novel experiments for melt crystal growth research. *IOP Conf. Ser.: Mater. Sci. Eng.* **2018**, *355*, 012001.

(22) Gilmer, G.; Bennema, P. Simulation of Crystal Growth with Surface Diffusion. *J. Appl. Phys.* **1972**, *43*, 1347.

(23) Saito, Y. *Statistical physics of crystal growth*; World Scientific: Singapore, 1998.

(24) Lutsko, J. F.; González-Segredo, N.; Durán-Olivencia, M. A.; Maes, D.; Van Driessche, A. E. S.; Sleutel, M. Crystal Growth Cessation Revisited: The Physical Basis of Step Pinning. *Cryst. Growth Des.* **2014**, *14*, 6129−6134.

(25) Lutsko, J. F.; Driessche, A. E. S. V.; Durán-Olivencia; Maes, D.; Sleutel, M. Step Crowding Effects Dampen the Stochasticity of Crystal Growth Kinetics. *Phys. Rev. Lett.* **2016**, *116*, 15501.

(26) Sleutel, M.; Lutsko, J.; Driessche, A. E. S. V. Mineral Growth beyond the Limits of Impurity Poisoning. *Cryst. Growth Des.* **2018**, *18*, 171.

(27) Chernov, A. A. Protein crystals and their growth. *J. Struct. Biol.* **2003**, *142*, 3−21.